Electrostatic Influence on Photoisomerization in Bacteriorhodopsin and Halorhodopsin

C. Punwong, a* S. Hannongbua, b and T. J. Martínez^{c,d*}

Department of Physics, Faculty of Science, Prince of Songkla University, Songkhla, 90112 Thailand

^bDepartment of Chemistry, Faculty of Science, Chulalongkorn University, Bangkok, 10330, Thailand

^cDepartment of Chemistry and the PULSE Institute, Stanford University, Stanford, CA, 94305 USA

^dSLAC National Accelerator Laboratory, Menlo Park, CA

email: *chutintorn@gmail.com, *todd.martinez@stanford.edu

Abstract

Bacteriorhodopsin (bR) and Halorhodopsin (hR) are both membrane proteins that

transport ions across the cell membrane in halobacteria. Their ion transport function is triggered

by photo-activated isomerization of the retinal protonated Schiff base (RPSB) chromophore. In

spite of their similar structures, bR and hR exhibit widely differing RPSB isomerization rates and

quantum yields (with bR being both faster and more efficient than hR). Previous simulations of

photoisomerization in bR and hR using ab initio multiple spawning (AIMS) with QM/MM have

successfully reproduced the experimentally-observed ordering of quantum yields and

isomerization rates, but the origin of these differences remains elusive. Here we investigate the

role of electrostatic interactions in the protein pocket surrounding RPSB. We probe the influence

of protein electrostatics by modifying the charge of the complex counterion in bR/hR to be

more/less negative than the native state. We find that such modifications lead to bR-like behavior

in hR and vice-versa. This demonstrates the crucial role of electrostatic interactions in

controlling the outcome of RPSB photoisomerization.

Introduction

Bacteriorhodopsin (bR) and Halorhodopsin (hR) are 7-helical membrane proteins containing all-*trans* retinal protonated Schiff base (RPSB) chromophore. Photo-activated isomerization of the chromophore to a 13-cis isomer induces conformational changes in both proteins to form a number of intermediates. These conformational changes lead to photo-driven ion-transport such that bR pumps H⁺ out of the cell and hR pumps Cl⁻ into the cell.

Both bR and hR are found on the cell membrane of Archaea such as *Halobacterium* salinarum, and share 31% sequence identity. Even though their structures are highly similar as shown in Figure 1, the two proteins lead to strikingly different RPSB isomerization rates and efficiencies. According to ultrafast spectroscopy experiments, the isomerization of RPSB in bR occurs in around 0.5 ps²⁻⁵ while in hR it takes several picoseconds. Moreover, the photoisomerization quantum yield in bR is 64%, 9-10 but only ~30% in hR. These observations indicate a crucial role of the protein environment, especially the chromophore binding pocket, in the photodynamics of RPSB. A detailed understanding of this role is prerequisite to rational design of photoactive proteins (for example through site-directed mutagenesis). 12-13

Recently we employed ab initio multiple spawning (AIMS) to simulate the excited state dynamics of bR and hR,¹⁴ using a hybrid quantum mechanical/molecular mechanical (QM/MM) description of the potential energy surfaces and nonadiabatic coupling matrix elements. We showed that this QM/MM AIMS approach successfully reproduces the differences in photoisomerization time scales and efficiencies for hR and bR. Our simulations led to a longer excited state lifetime in hR (bi-exponential: 0.2/5.34 ps) compared to bR (single-exponential: 0.62 ps) and a smaller isomerization quantum yield in hR compared to bR (50% vs. 70%).¹⁴ For comparison, the experimentally determined excited state lifetime is 1.5/6.6ps (biexponential) for bR and 0.5ps (monoexponential) for bR. The experimentally determined isomerization quantum

yields are 0.3/0.64 for hR/bR, respectively. There is a long history of both theoretical^{12, 15-17} and experimental¹⁸⁻¹⁹ indications that electrostatic effects might influence the isomerization rate in photoactive proteins. Here, we quantify this for bR and hR through comprehensive analysis of our previous simulations on the native proteins and through additional simulations of excited state dynamics where the charge of the RPSB complex counterion (we consider the "complex counterion" to be the negatively charged moieties and H-bonded water molecules closest to the protonated Schiff base, e.g. aspartate residues (D85 and D212), and the water molecule which is H-bonded to both of these in bR or D238, Cl⁻ and the water molecule which is H-bonded to both of these in hR as shown in Figure 2) is modified. Our calculations show that the behavior of bR can be modified to be more like hR (and vice versa) through modification of the charge of the complex counterion. This provides insight into the role of electrostatics in controlling the photoisomerization dynamics.

Methods

Dynamics simulations of bR and hR with charge modifications for the RPSB complex counterion

We previously proposed that one of the important roles of complex counterion in the binding site is to suitably stabilize the positive charge on the chromophore Schiff base. ¹⁴ On the excited state (S₁), the positive charge can delocalize from the Schiff base side to the β -ionone side of the retinal chromophore. This charge redistribution facilitates isomerization at the C₁₃=C₁₄ bond. In hR the negatively charged moieties in the complex counterion are mostly closer to the Schiff base than in bR. The resulting increased electrostatic attraction impedes migration of the positive charge from the Schiff base towards the β -ionone ring. In our previous work, we identified this slowdown in charge migration with the slowdown in isomerization. ¹⁴ In this work,

we will modify the charge on the RPSB counterion and observe the resulting changes in the rate of charge migration. If our hypothesis connecting the charge migration and isomerization rates is correct, we should thereby be able to increase the isomerization rate in hR and/or decrease the isomerization rate in bR. We carry out this test here by artificially modifying the charges of D85 in bR and Cl⁻ in hR. Both D85 and Cl⁻ are part of the Schiff base's complex counterion and located at approximately the same position in each protein as shown in Figure 2. We set the charge of the Cl⁻ ion to be 0.5e more positive for simulations of modified hR (hR+0.5e). This modification is expected to lessen the Coulomb attraction from Cl⁻ and thereby facilitate migration of the positive charge. For our simulations of modified bR, we decreased the charge of D85 by 0.5e, distributing the extra negative charge (-0.5e) equally on the two oxygen atoms of its carboxylate sidechain (bR-0.5e). This modification is expected to increase the Coulomb attraction and retard charge migration.

As our goal is to probe the relationship between charge migration and isomerization, we wanted to avoid as much as possible any significant conformational changes that might occur because of the modified charges. It is also critical to avoid any rearrangements in the hydrogen bonding network around the chromophore, as this has been shown^{18, 20-24} to play a critical role in the photoisomerization. Thus, we start the simulations of the modified proteins from the same initial conditions we used previously¹⁴ for bR and hR – these were determined through dynamical sampling of the native proteins on the ground electronic state (i.e. without any modifications to the Cl⁻ or D85 charges). In this way, we ensure that the positions of key residues as well as the hydrogen bond network in the chromophore's binding site are as close as possible to the native state and our results reflect primarily the effects of the charge modification on the excited state dynamics.

Ab initio multiple spawning (AIMS) dynamics

The photo-activated dynamics of RPSB in bR-0.5e and hR+0.5e are simulated using *ab initio* multiple spawning (AIMS),²⁵⁻²⁷ which simultaneously solves the electronic Schrödinger equation and the nuclear equations of motion, i.e. "on-the-fly" dynamics including quantum effects such as electronic transitions at conical intersections and curve crossings. The electronic structure calculations provide not only the potential energies and their gradients but also the nonadiabatic coupling matrix elements. The nuclear wave function is expressed as a linear combination of frozen Gaussians travelling on their specific electronic states. Each of these "trajectory basis functions" (TBFs) evolves classically on a given adiabatic potential energy surface (PES). When the gap between electronic states becomes small, new TBFs are "spawned" on coupled electronic states. The nuclear Schrodinger equation is solved in the time-evolving basis set of TBFs in order to determine the population of each TBF, i.e. to describe nonadiabatic transitions. AIMS has been implemented in several electronic structure program suites such as MOLPRO,²⁸⁻²⁹ MOPAC,³⁰⁻³¹ and GAMESS.³²⁻³³ A more detailed discussion can be found in previous publications.^{25-27, 29, 34}

As discussed above, the initial positions and momenta for each TBF are obtained by sampling from ground state dynamics of bR/hR. For ease of comparison with previous simulations of the native proteins, we choose exactly the same initial conditions as used in previous work.¹⁴ Ten independent simulations (each starting with a single TBF on the excited electronic state) are carried out for each system. From twenty simulations of native bR, the isomerization time ranges from 0.16 to 1.6 ps, with an average of 0.67 ps.¹⁴ We selected ten of these twenty initial conditions for simulations with the modified charge. We purposely chose the ten fastest isomerizing trajectories for dynamics of bR-0.5e in order to accentuate the effect of modifying the charge (which we hypothesize to retard the isomerization in bR). For native hR,

the lifetime was biexponential, with both fast and slow components. Again, in order to accentuate the effect of modifying the charge (which we hypothesize to lead to faster isomerization for hR), we choose the slowest ten initial conditions (isomerizing in 1.5-7.2ps in native hR) for our simulations of hR+0.5e. These correspond to the slow component of isomerization in hR. When we compare to results for bR and hR, we also consider these restricted sets of initial conditions, i.e. only the fastest isomerizing bR initial conditions and the slowest isomerizing hR initial conditions (the full results for hR and bR are available in our previous work). A fourth-order Runge-Kutta scheme³⁵ is used with a 0.5 fs time step to integrate the equations of motion for the classical trajectories and complex amplitudes. The PESs and the nonadiabatic couplings necessary for the AIMS simulations are provided by the QM/MM method described below. All atoms in the protein and chromophore are allowed to move without constraint. Each TBF begins on S₁ and the dynamics is followed until more than 99% of the population has reached the ground electronic state (S₀) or until 12.5 ps, whichever comes first.

Hybrid QM/MM method

As in our previous work, the QM/MM method³⁶⁻³⁷ is employed for the calculations of PESs and the nonadiabatic coupling matrix elements. For all calculations (bR and hR) discussed herein, the RPSB chromophore (54 atoms) is modeled quantum mechanically while the rest of the protein is treated with a classical molecular force field. The QM region is described with a reparameterized multireference semiempirical configuration interaction method,³⁸ where the PM3 parameter set has been reoptimized for RPSB by fitting to *ab initio* CASSCF results at a few key geometries.³⁹ The PESs for torsional rotation about various C=C bonds of RPSB using the reoptimized parameters show excellent agreement with *ab initio* CASPT2⁴⁰ results using an active space containing all π electrons.¹⁷ This new parameter set has proven robust for

simulating excited state dynamics of RPSB in various environments. ^{14, 17, 41} The semiempirical QM region is modeled with a floating occupation molecular orbital/complete active space configuration interaction (FOMO-CASCI) wave function. ⁴² In FOMO calculations, molecular orbitals are optimized at a fixed (and finite) electronic temperature, resulting in fractional occupation numbers. A complete active space configuration interaction (CASCI) is then performed with these optimized molecular orbitals to obtain the electronic energies for the desired states. The FOMO-CASCI approach is implemented in a development version of the semiempirical program package MOPAC2000. ³⁰ The FOMO-CASCI for RPSB is performed with an active space of six electrons in six orbitals and the broadening parameter (related to the electronic temperature) is set to 0.2 atomic units.

Except where noted, we follow the same simulation setup as our previous work¹⁴ on bR and hR. For bR, we start with the crystal structure (1C3W, resolved at 1.55 Å).⁴³ Missing residues 157-161 are added based on the template of residues 156-164 from another bR structure (1QHJ, resolved at 1.9 Å).⁴⁴ For bR, all titratable residues are charged conforming to their normal protonation state at pH 7, except for D96, D115, and E204, which experiments have found to be protonated (neutral).⁴⁵⁻⁴⁶ Finally, the net charge of D85 is artificially set to -1.5e as described above in order to create bR-0.5e. The RPSB chromophore (QM part) and the protein (MM part) are covalently bound through C_{δ} of K216. We use a connection atom scheme⁴⁷⁻⁴⁸ to describe the QM-MM covalent interaction using a special set of semiempirical parameters for the connection atom.⁴⁸ The MM region is treated with the AMBER94 forcefield.⁴⁹⁻⁵²

The hR geometry is modeled from the 1E12 X-ray structure.¹ The protonation state at pH 7 is assigned for all acidic and basic residues except for H95 which is charged (protonated) according to experimental results on hR mutants.⁵³ The Cl⁻ ion charge is set to +0.5e to create

hR+0.5e. The RPSB chromophore binds covalently to the protein at C_{δ} of K242. The same AMBER94 forcefield⁴⁹⁻⁵² and connection parameters⁴⁸ are used as in bR.

For both bR-0.5e and hR+0.5e (and our previous simulations of the native bR and hR), the proteins are modeled in isolation without accounting for the surrounding membrane. This is expected to be sufficient for our investigations because 1) both membrane and vacuum environments have low dielectric and 2) we are only interested in the short-time (≈10 ps) dynamics connected with the earliest isomerization events.

Free energy calculations

We used umbrella sampling to estimate free energy profiles along torsion angle about the RPSB C₁₃=C₁₄ bond.⁵⁴⁻⁵⁵ Constrained dynamics simulations are performed (C₁₃=C₁₄ torsion angle constrained in 10° increments from 0-180° with a force constant of 100 kcal/mol for the bias potential) for each window. In each window, the system is first equilibrated on S₁ at 298K with 1ps of Brownian dynamics using a friction coefficient of 0.1 fs⁻¹. A further 2ps of constrained dynamics on S₁ is used to obtain statistics for umbrella sampling. Finally, the probability distribution and free energy profile are calculated with WHAM.⁵⁶

Results and Discussion

Table 1 summarizes the results from the dynamics simulations. The "isomerization starting time" is the average time for the first spawning or population transfer event, which coincides with $\sim 90^{\circ}$ torsion about the $C_{13}=C_{14}$ bond of RPSB. This 90°-twisted conformation is approximately at the conical intersection where the energy gap between S_1 and S_0 vanishes. Once this region is reached, a new TBF is generated on the ground state. As a result of spawning, the excited state population is transferred multiple times (6 on average) within 200 fs from the first spawning until there is less than 1% left. Once it is on the ground electronic state, the spawned

TBF either isomerizes successfully to the 13-cis conformer or returns back to its original alltrans conformation. The fraction of the population in 13-cis state (averaged over all initial conditions) is the average isomerization quantum yield reported in Table 1. Contributions to the isomerization quantum yield are determined after each TBF evolves on S₀ for 500 fs. Detailed analysis of the TBFs shows that this is sufficient to determine the cis or trans conformation (about the C₁₃=C₁₄ bond) of the ground state RPSB product. We remind the reader that the results for native hR and bR are selectively taken from previous simulations in order to emphasize the results of modifying the counterion complex charge. ¹⁴ Therefore, the excited state lifetime and isomerization quantum yield for native bR and hR reported in Table 1 are meant for comparison purposes only. The simulation predictions for these values in bR and hR given in Table 1 represent a worst case comparison for our hypothesis connecting charge migration and isomerization – they are not a prediction for bR/hR. Since we have selected only the fastest isomerizing bR initial conditions, the excited stated lifetime of bR in this work is decreased from 0.62 ps¹⁴ to 0.26 ps. Since we selected only the slowest isomerizing initial conditions in hR, the bi-exponential decay (0.2/5.34 ps)¹⁴ becomes a single exponential decay with a time constant of 3.86 ps. These results can now be compared with the charge-modified proteins. As shown in Table 1, isomerization is accelerated 8-fold in hR+0.5e compared to native hR (0.5 ps vs. 4.1 ps). The faster isomerization rate almost matches the rate of native bR (recall that we have selected the *slowest* isomerizing initial conditions from hR). Additionally, the isomerization quantum yield of hR+0.5e increases relative to native hR (63% compared to 50%, respectively). Lowering the negative charge of Cl enhances the isomerization rate and efficiency in hR. Thus, hR behaves more like bR when the electrostatic environment is altered to favor migration of the positive charge along the RPSB backbone.

In comparison, for bR-0.5e, isomerization is not observed at all within 12.5 ps after photoexcitation. Recall that these are the *fastest* isomerizing initial conditions for bR, so it is very clear that retarding the migration of positive charge (by making the complex counterion more negative) slows down isomerization. As illustrated in Figure 3, the excited state population decays of the four systems can be roughly separated into two groups; one is the fast decay comprising bR and hR+0.5e, and the other is slow decay comprising hR and bR-0.5e. More specifically, the excited state population in both hR+0.5e and bR is almost completely transferred to the ground state within 1 ps. Although the lifetime of hR+0.5e has two components, over 74% of the population decays with the faster time constant (0.2 ps). The results from hR+0.5e and bR-0.5e simulations clarify the important role of electrostatic interactions with RPSB exerted by the complex counterion.

Role of electrostatic interactions in photoisomerization of bR and hR

The charge modifications we considered do not alter the bond selectivity of isomerization but they do lead to dramatic changes in the isomerization time scale. We focus on the negatively charged moieties (D85/D212 and D238/Cl⁻ in bR/hR, respectively) in order to better understand this influence. In both bR and hR, there is also a water molecule bridging the two negative moieties through hydrogen bonding. The two negative moieties and the bridging water molecule are part of a pentagonal hydrogen bonding network that is clearly visible in Figure 2.

We focus first on the charge distribution in RPSB during the dynamics. In both native and charge-modified conditions, the positive charge which starts out on the Schiff base side (N_z -side) of the C_{13} = C_{14} bond migrates to the β -ionone side during the S_1 dynamics. This is demonstrated in the left panel of Figure 4, which shows the time-evolution of the sum of charges on the N_z -side of RPSB for all four cases (bR, bR-0.5e, hR, hR+0.5e), averaged over all initial

conditions. At the start of the dynamics (and during the first 300fs after photoexcitation), the positive charge is least strongly localized on the Schiff base in bR and hR+0.5e compared to hR and bR-0.5e. The positive charge also migrates fastest in bR and hR+0.5e, which are the two fastest isomerizing cases. This demonstrates the correlation of positive charge migration rate and isomerization rate. In the right panel of Figure 4, we show how the positive charge migration is related to the torsional coordinate of RPSB (for data points sampled from the excited state dynamics). This figure also shows that positive charge migration is correlated with twisting about the C₁₃=C₁₄ bond. The correlation is least visible in bR-0.5e, at least in part because RPSB does not isomerize over the simulated time period in this case. The variation of the RPSB charge distribution on S₀ and S₁ has been reported previously in both experimental and theoretical work.^{23, 57-63} On the ground state, the covalent state character is dominant, stabilizing the positive charge at the Schiff base of RPSB. 64-68 On the excited state however, charge delocalization or charge transfer character is favored.⁶⁴⁻⁶⁸ The excited state local minimum geometry is when a double bond is 90°-twisted which is mostly analogous to the conical intersection geometry. Destabilization of the positive charge on the Schiff base side allows for delocalization and/or migration of the positive charge to the β -ionone ring on S_1 . This is accompanied by isomerization that leads to the conical intersection geometry that promotes transitions back to the ground state. Thus charge transfer within the chromophore is crucial to reach the twisted conical intersection and return to the ground state.¹⁴ To the extent that a surrounding electric field can disfavor this charge transfer, the isomerization rate will be diminished. A similar role for the electric field has also been suggested in green fluorescent protein (GFP), where protein electrostatics control photoisomerization of the GFP chromophore. ¹⁶

On the ground state, the positive charge at the Schiff base side of RPSB is maintained by the complex counterion through the electrostatic interaction. However, such electrostatic interactions must be lessened on the excited state for positive charge relocation. Following our previous work, 14 we measure the distances between the Schiff base and the three members of the complex counterion to characterize the strength of electrostatic interactions during S₁ dynamics. Five distances from the protonated Schiff base to these negatively charged atoms in bR and bR-0.5e are chosen and labeled in Figure 2. In hR and hR-0.5e, only four distances are measured since two oxygen atoms of D85 in bR are replaced by one Cl. As shown in Figure 5, the distances in the charge-modified proteins are quite similar to those in the native one except the distance from the Schiff base to D85/Cl⁻ in bR/hR. Due to its greater negative charge in bR-0.5e, D85 gets closer (~1 Å) to the positively charged Schiff base when compared to bR. On the contrary, since Cl⁻ becomes less negative in hR+0.5e, it moves away (~1 Å) from the Schiff base. Interestingly, the increase of the Cl⁻ distance in hR+0.5e is similar to the increase of D85 distance in bR within 200-300 fs, which is also the isomerization time scale in both systems. This dislocation of the negatively charged moieties away from the Schiff base indicates lower electrostatic attraction, which favors positive charge migration in RPSB on S₁. Figure 6 shows the total electrostatic potential exerted by the three moieties comprising the complex counterion, measured at the Schiff base hydrogen atom. The Coulomb potential is calculated from the charges and distances of atoms in the carboxylate group of aspartate residues (or Cl- in case of hR and hR+0.5e), and the associated water molecule. The potential is most attractive in the case of bR-0.5e, consistent with the strong stabilization of the positive charge on the Schiff base that prevents isomerization. The variation in the electrostatic potential for bR, hR, and hR+0.5e is

less dramatic, but the ordering reflects the observed isomerization rates – the lesser attraction for positive charge at the Schiff base hydrogen atom leads to a faster isomerization rate.

The electrostatic influence of the complex counterion on RPSB photoisomerization in bR and hR is schematically presented in Figure 7. Making the counterion more negative (bR-0.5e compared to bR, left panel) stabilizes the positive charge on the Schiff base due to Coulombic attraction. As the chromophore isomerizes, the positive charge migrates to the β-ionone ring side of the chromophore. This charge migration is disfavored when the counterion has been made more negative, thereby also disfavoring torsion and slowing isomerization. On the other hand, making the counterion less negative (hR+0.5e compared to hR, right panel), favors positive charge migration towards the β-ionone ring. Hence the barrier to isomerization is lowered and isomerization is accelerated. We indeed observe the change in free energy barriers performed by umbrella sampling⁵⁴⁻⁵⁵ with WHAM.⁵⁶ The barrier increases by 2.6 kcal/mol going from bR to bR-0.5e, while the barrier decreases by 1.0 kcal/mol going from hR to hR+0.5e. These results predict that the excited state lifetime of bR is 81x longer in bR-0.5e compared to bR. Similarly, for hR, the S₁ lifetime is predicted to be 5.4x shorter in hR+0.5e compared to hR. This trend agrees well with our direct dynamics simulations.

Conclusions

We investigated the way in which RPSB-counterion electrostatic interactions determine the photoisomerization rates in bR and hR. We compared AIMS-QM/MM dynamics simulations of native bR and hR with simulations that artificially modified the charge of the complex counterion (referred to as bR-0.5e and hR+0.5e). We showed that making the charge of the counterion more/less negative slows down/speeds up isomerization, respectively. These results suggest that the isomerization timescale (and hence also the excited state lifetime) is strongly

influenced by the timescale for migration of the positive charge along the RPSB backbone. In hR+0.5e, the isomerization of RPSB is dramatically faster than in hR (540 fs vs. 4 ps) with a small increase in quantum yield. On the other hand, no isomerization is observed in bR-0.5e during the 12.5 ps simulations while isomerization in bR occurs at about 300 fs. These results indicate a crucial influence of the charged/polar moieties near the Schiff base in the photochemistry of RPSB.

Our goal in this work has not been to provide quantitative predictions for the isomerization quantum yield and excited state lifetime in bR and hR. Such quantitative predictions are best achieved by direct simulation, which we have previously performed. Unfortunately, agreement between theory and experiment does not automatically lead to any better understanding. Our focus in this paper has been to gain deeper insight into the origins of the experimental and theoretical observed differences. Thus, we modified the charges in bR and hR in a manner which might exaggerate the electrostatic potential differences in bR and hR. The complete lack of isomerization on the 10ps timescale in bR-0.5e is evidence that the resulting electrostatic potential modifications are more extreme than those in the wild-type proteins. At the same time, this clarifies the effect of changes in the electrostatic potential in the region surrounding the RPSB chromophore.

Following our previous work on wild-type bR and hR photodynamics, we also analyzed the charge-modified proteins by calculating the counterion-RPSB distances and the electrostatic potential generated by the counterion at the Schiff base hydrogen atom. These results confirm the correlation between electrostatic stabilization preventing positive charge migration from the Schiff base to the β-ionone ring side of the chromophore and deceleration of the excited state isomerization. These results predict that the isomerization rate in bR and hR can be

accelerated/decelerated by any mutation which increases/decreases the propensity for positive charge migration along the RPSB backbone.

Acknowledgements

This work (grant number MRG5380268 and TRG5780300) is jointly supported by the Thailand Research Fund, Thailand's Office of the Higher Education Commission, Faculty of Science, Prince of Songkla University, and the National Science Foundation (CHE-1740645). This work used the XStream computational resource supported by the NSF MRI program (Grant No. ACI-1429830) as well as computational facilities at the Department of Physics, Prince of Songkla University.

Supporting Information for Publication

Atomic partial charges of D85 in the simulations of bR (using default AMBER charges) and of bR-0.5e (using modified charges), Coulomb potential exerted on the Schiff base hydrogen atom by each member of the complex counterion.

Table 1. Average isomerization starting time, excited state lifetime, and isomerization quantum yield (fraction of S_0 population in 13-cis configuration) of all-*trans* RPSB in hR and bR. Error bars are determined by bootstrapping.⁶⁹

Protein	Isomerization	Excited State	Isomerization
	Starting Time	Lifetime	Quantum Yield
bR	0.30±0.03 ps	0.26 ps	0.70 ± 0.07
hR	4.14±0.72 ps	3.86 ps	0.50 ± 0.08
bR-0.5e	> 12.5 ps	-	-
hR+0.5e	$0.54\pm0.22 \text{ ps}$	0.2/1.43 ps	0.63 ± 0.09

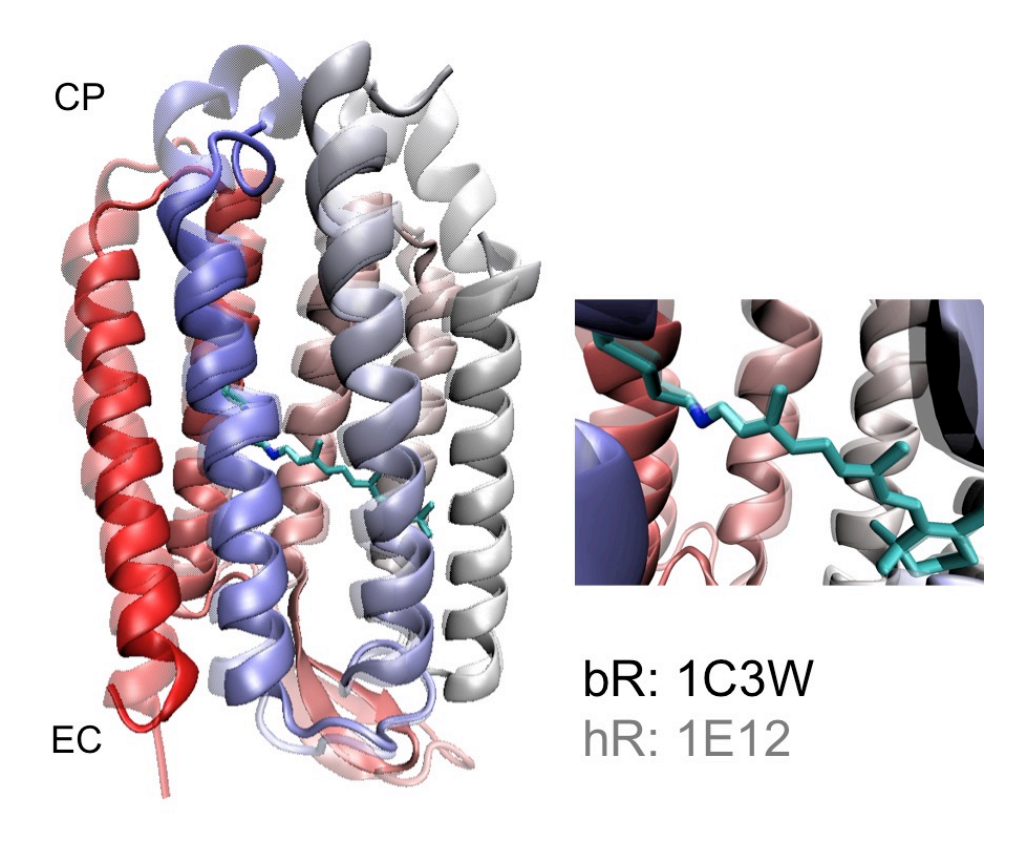


Figure 1. The left panel shows a superposition of bR (opaque representation) and hR (transparent representation) X-ray crystal structures. CP and EC are cytoplasmic and extracellular sides of cell membrane, respectively. The right panel shows a zoom-in of the proteins to reveal the RPSB chromophore in stick representation.

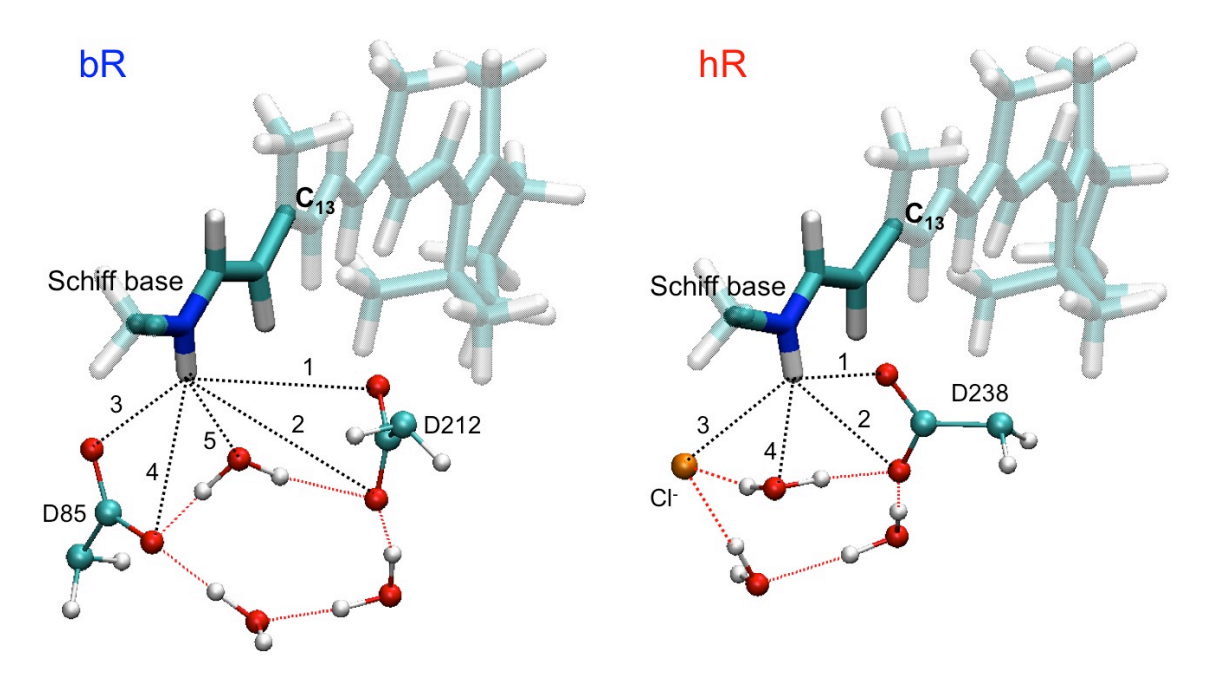


Figure 2. The pentagonal H-bond networks in dotted red lines of bR (left) and hR (right). The H-bonds from the Schiff base of RPSB in black dotted lines are labeled for distance analysis.

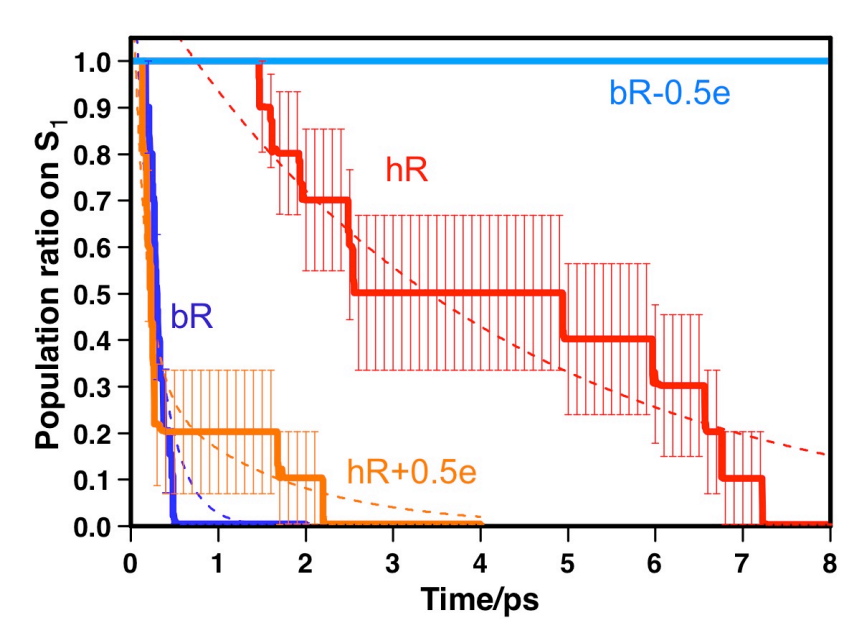


Figure 3. Average (from 10 selected trajectories) excited state population decays of RPSB in hR (red) and bR (blue). The average from the associated simulations of each protein with artificially modified charges are in light blue/orange for bR-0.5e/hR+0.5e, respectively. Thin dashed lines are exponential fits. Error bars are given as standard error of the mean.

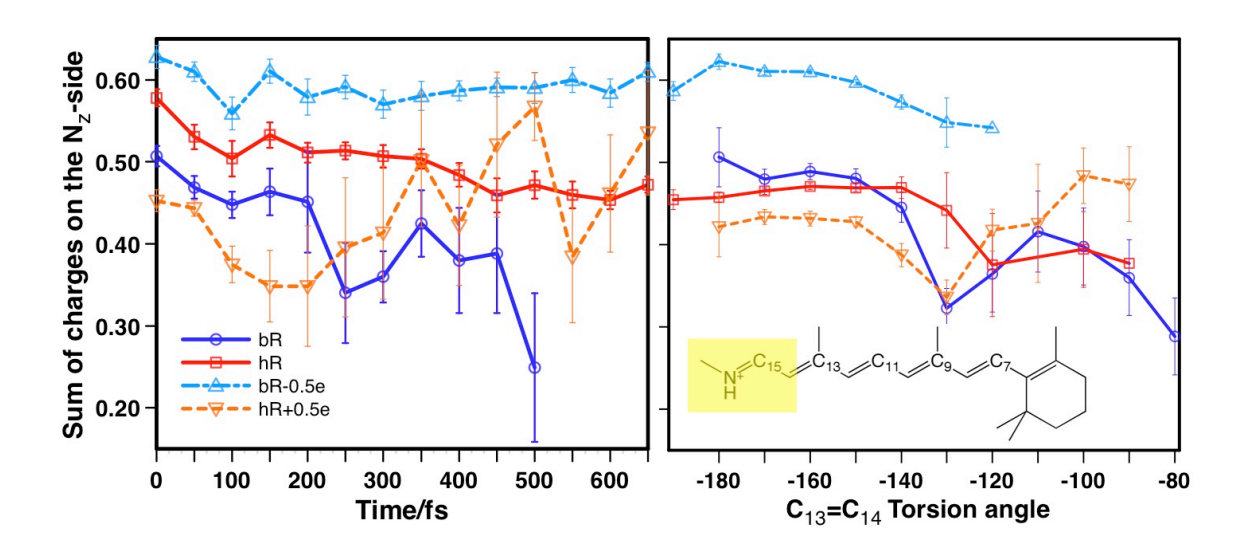


Figure 4. Time dependence (left panel) and torsional dependence (right panel) of the charge on the Schiff base side (N_z-side, highlighted in yellow in the inset) for bR (blue), hR (red), bR-0.5e (dot-dashed light blue), and hR+0.5e (dashed orange). Charges are summed over all atoms on Schiff base side of RPSB and averaged over all ten initial TBFs on the excited state of each protein. Error bars represent standard error of the mean.

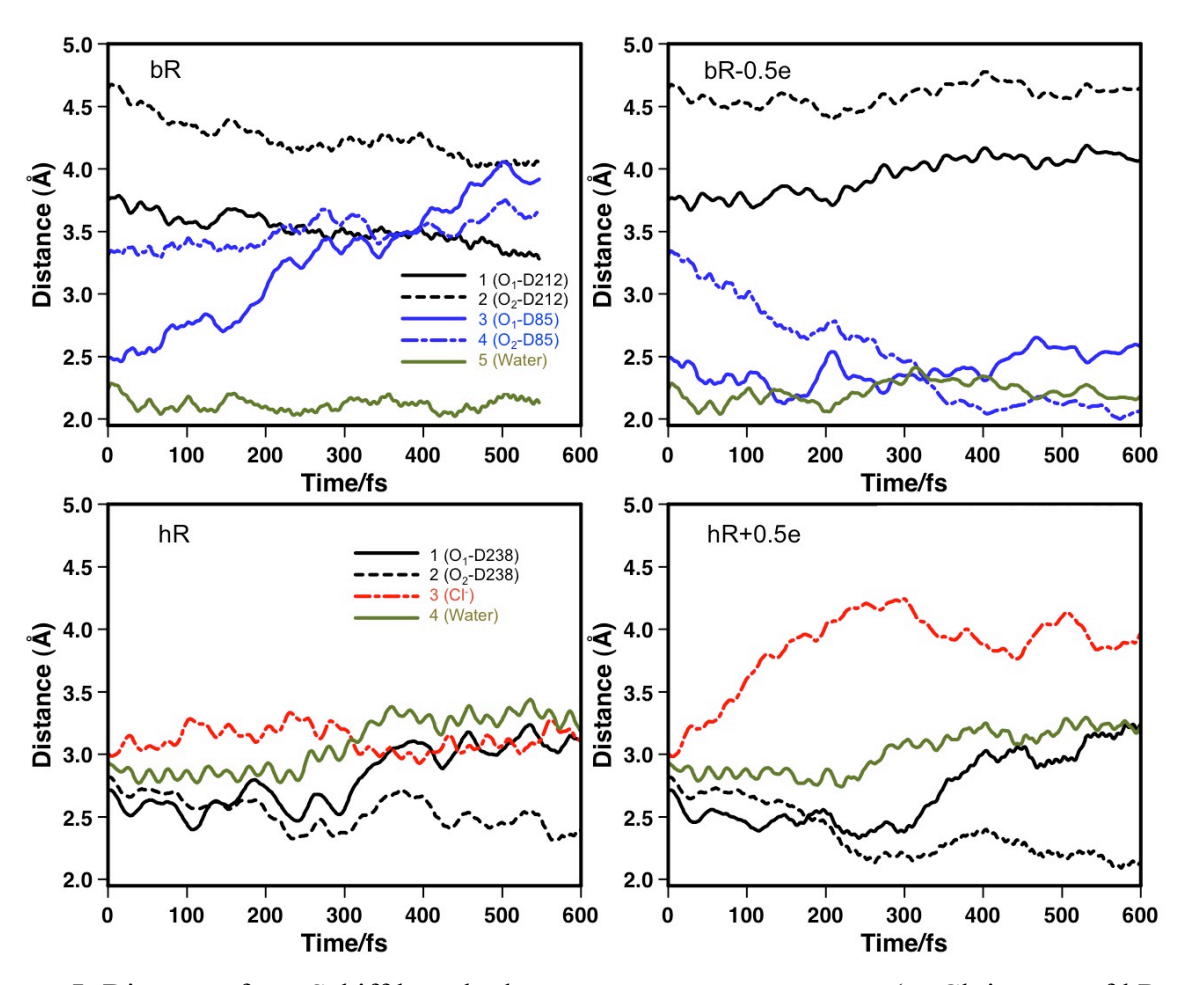


Figure 5. Distances from Schiff base hydrogen atom to oxygen atoms (or Cl⁻ in case of hR and hR+0.5e) belonging to the three members of the complex counterion (numbering follows Figure 2). The top left and right panels show the distances in the case of bR and bR-0.5e, respectively. The bottom left and right panels show the distances in the case of hR and hR+0.5e. Note that D238 and the Cl⁻ ion in hR are equivalent to D212 and D85 in bR. The results are averaged over ten TBFs from excited state simulations of each protein.

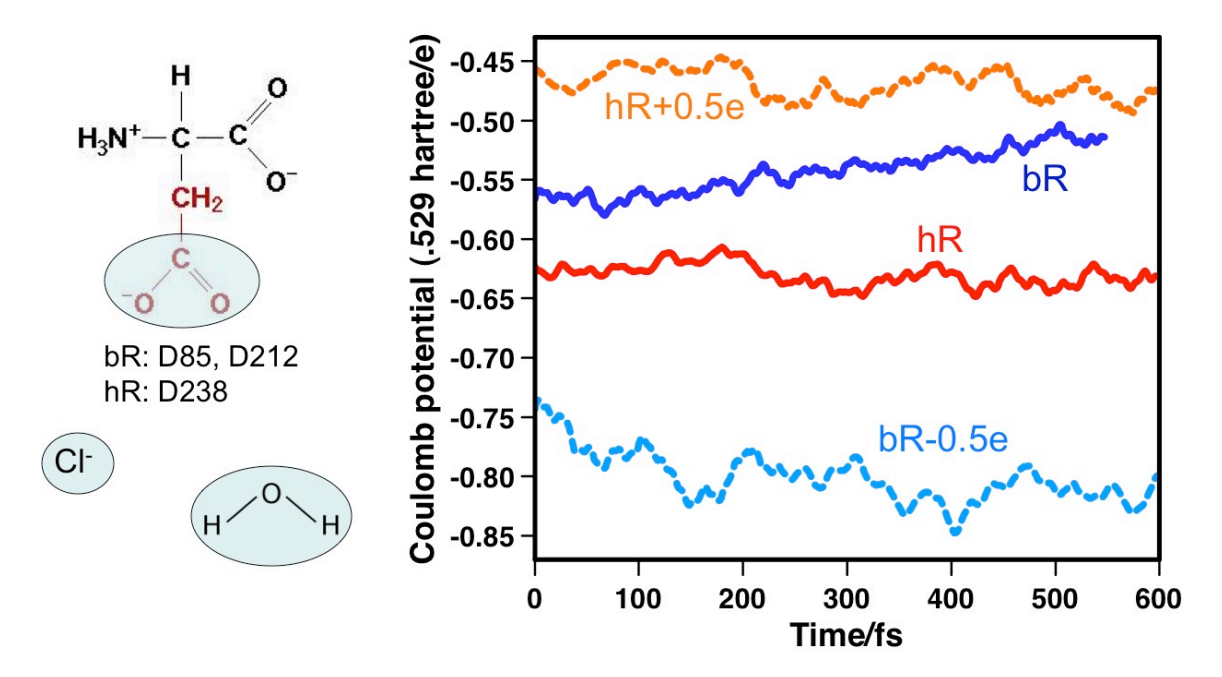


Figure 6. Total electrostatic potential generated by three members of complex counterion at the Schiff base hydrogen atom. The potential is calculated from the charges and distances of atoms in the carboxylate group of aspartate residues, Cl⁻, and the bridging water molecule as indicated by circling in the left panel. For bR (solid blue) and bR-0.5e (dashed light blue), the computed potential reflects the influence of D85, D212 and the bridging water molecule. For hR (solid red) and hR+0.5e (dashed orange), the computed potential is due to Cl⁻, D238 and the bridging water molecule. Results are averaged over ten TBFs from each protein.

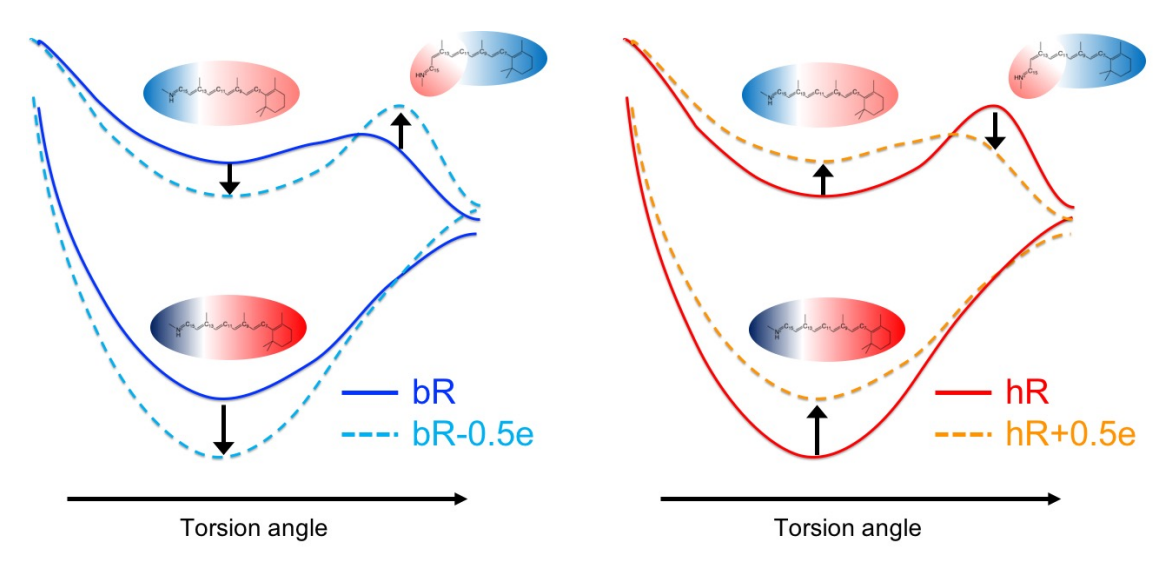


Figure 7. Schematic energy diagrams showing the influence of electrostatics on photoisomerization of RPSB in native bR (solid blue line) and bR-0.5e (dashed light blue line) in the left panel, in hR native hR (solid red line) and hR+0.5e (dashed orange line) in the right panel. The charge distribution of RPSB is approximately represented with gradient colors where blue and red show positive and negative charges, respectively. Changes in the potential arising from charge modifications are indicated by up/down arrows.

References

- 1. Kolbe, M.; Besir, H.; Essen, L. O.; Oesterhelt, D., Structure of the Light-Driven Chloride Pump Halorhodopsin at 1.8 Angstrom Resolution. *Science* **2000**, *288*, 1390-1396.
- 2. Petrich, J. W.; Breton, J.; Martin, J. L.; Antonetti, A., Femtosecond Absorption Spectroscopy of Light-Adapted and Dark-Adapted Bacteriorhodopsin. *Chem. Phys. Lett.* **1987**, *137*, 369-375.
- 3. Dobler, J.; Zinth, W.; Kaiser, W.; Oesterhelt, D., Excited-State Reaction Dynamics of Bacteriorhodopsin Studied by Femtosecond Spectroscopy. *Chem. Phys. Lett.* **1988**, *144*, 215-220.
- 4. Mathies, R. A.; Cruz, C. H. B.; Pollard, W. T.; Shank, C. V., Direct Observation of the Femtosecond Excited-State Cis-Trans Isomerization in Bacteriorhodopsin. *Science* **1988**, *240*, 777-779.
- 5. Herbst, J.; Heyne, K.; Diller, R., Femtosecond Infrared Spectroscopy of Bacteriorhodopsin Chromophore Isomerization. *Science* **2002**, *297*, 822-825.
- 6. Peters, F.; Herbst, J.; Tittor, J.; Oesterhelt, D.; Diller, R., Primary Reaction Dynamics of Halorhodopsin, Observed by Sub-Picosecond Ir Vibrational Spectroscopy. *Chem. Phys.* **2006**, *323*, 109-116.
- 7. Kandori, H.; Yoshihara, K.; Tomioka, H.; Sasabe, H., Primary Photochemical Events in Halorhodopsin Studied by Subpicosecond Time-Resolved Spectroscopy. *J. Phys. Chem.* **1992**, *96*, 6066-6071.
- 8. Arlt, T.; Schmidt, S.; Zinth, W.; Haupts, U.; Oesterhelt, D., The Initial Reaction Dynamics of the Light-Driven Chloride Pump Halorhodopsin. *Chem. Phys. Lett.* **1995**, *241*, 559-565.
- 9. Logunov, S. L.; ElSayed, M. A.; Song, L.; Lanyi, J. K., Photoisomerization Quantum Yield and Apparent Energy Content of the K Intermediate in the Photocycles of Bacteriorhodopsin, Its Mutants D85n, R82q, and D212n, and Deionized Blue Bacteriorhodopsin. *J. Phys. Chem.* **1996**, *100*, 2391-2398.
- 10. Tittor, J.; Oesterhelt, D., The Quantum Yield of Bacteriothodopsin. *FEBS Lett.* **1990**, 263, 269-273.

- 11. Oesterhelt, D.; Hegemann, P.; Tittor, J., The Photocycle of the Chloride Pump Halorhodopsin. 2. Quantum Yields and a Kinetic Model. *EMBO J.* **1985**, *4*, 2351-2356.
- 12. Martinez, T. J., Insights for Light-Driven Molecular Devices from Ab Initio Multiple Spawning Excited-State Dynamics of Organic and Biological Chromophores. *Acc. Chem. Res.* **2006**, *39*, 119-126.
- 13. Gozem, S.; Melaccio, F.; Luk, H. L.; Rinaldi, S.; Olivucci, M., Learning from Photobiology How to Design Molecular Devices Using a Computer. *Chem. Soc. Rev.* **2014**, *43*, 4019-4036.
- 14. Punwong, C.; Martínez, T. J.; Hannongbua, S., Direct Qm/Mm Simulation of Photoexcitation Dynamics in Bacteriorhodopsin and Halorhodopsin. *Chem. Phys. Lett.* **2014**, *610–611*, 213-218.
- 15. Cembran, A.; Bernardi, F.; Olivucci, M.; Garavelli, M., The Retinal Chromophore/Chloride Ion Pair: Structure of the Photo Isomerization Path and Interplay of Charge Transfer and Covalent States. *Proc. Natl. Acad. Sci. U. S. A.* **2005**, *102*, 6255-6260.
- 16. Park, J. W.; Rhee, Y. M., Electric Field Keeps Chromophore Planar and Produces High Yield Fluorescence in Green Fluorescent Protein. *J. Am. Chem. Soc.* **2016**, *138*, 13619-13629.
- 17. Punwong, C.; Owens, J.; Martinez, T. J., Direct Qm/Mm Excited-State Dynamics of Retinal Protonated Schiff Base in Isolation and Methanol Solution. *J. Phys. Chem. B* **2015**, *119*, 704-714.
- 18. Song, L.; Elsayed, M. A.; Lanyi, J. K., Protein Catalysis of the Retinal Subpicosecond Photoisomerization in the Primary Process of Bacteriorhodopsin Photosynthesis. *Science* **1993**, *261*, 891-894.
- 19. Song, L.; ElSayed, M. A.; Lanyi, J. K., Effect of Changing the Position and Orientation of Asp85 Relative to the Protonated Schiff Base within the Retinal Cavity on the Rate of Photoisomerization in Bacteriorhodopsin. *J. Phys. Chem.* **1996**, *100*, 10479-10481.
- 20. Nina, M.; Roux, B.; Smith, J. C., Functional Interactions in Bacteriorhodopsin: A Theoretical Analysis of Retinal Hydrogen Bonding with Water. *Biophys. J.* **1995**, *68*, 25-39.
- 21. Kandori, H.; Belenky, M.; Herzfeld, J., Vibrational Frequency and Dipolar Orientation of the Protonated Schiff Base in Bacteriorhodopsin before and after Photoisomerization. *Biochemistry* **2002**, *41*, 6026-6031.

- 22. Rajamani, R.; Gao, J., Combined Qm/Mm Study of the Opsin Shift in Bacteriorhodopsin. *J. Comp. Chem.* **2002**, *23*, 96-105.
- 23. Altoe, P.; Cembran, A.; Olivucci, M.; Garavelli, M., Aborted Double Bicycle-Pedal Isomerization with Hydrogen Bond Breaking Is the Primary Event of Bacteriorhodopsin Proton Pumping. *Proc. Natl. Acad. Sci. U. S. A.* **2010**, *107*, 20172-7.
- 24. Muroda, K.; Nakashima, K.; Shibata, M.; Demura, M.; Kandori, H., Protein-Bound Water as the Determinant of Asymmetric Functional Conversion between Light-Driven Proton and Chloride Pumps. *Biochemistry* **2012**, *51*, 4677-4684.
- 25. Ben-Nun, M.; Quenneville, J.; Martinez, T. J., Ab Initio Multiple Spawning: Photochemistry from First Principles Quantum Molecular Dynamics. *J. Phys. Chem. A* **2000**, *104*, 5161-5175.
- 26. Ben-Nun, M.; Martínez, T. J., Ab Initio Quantum Molecular Dynamics. *Adv. Chem. Phys.* **2002**, *121*, 439-512.
- 27. Curchod, B. F. E.; Martinez, T. J., Ab Initio Nonadiabatic Quantum Molecular Dynamics. *Chem. Rev.* **2018**, *118*, 3305-3336.
- 28. Werner, H. J.; Knowles, P. J.; Lindh, R.; Schuetz, M.; Celani, P.; Korona, T.; Manby, F. R.; Rauhut, G.; Amos, R. D.; Bernhardsson, A.; et al. *Molpro*, 2006.1; 2006.
- 29. Levine, B. G.; Coe, J. D.; Virshup, A. M.; Martinez, T. J., Implementation of Ab Initio Multiple Spawning in the Molpro Quantum Chemistry Package. *Chem. Phys.* **2008**, *347*, 3-16.
- 30. Stewart, J. J. P. Mopac 2000, Fujitsu Limited: Tokyo, Japan, 1999.
- 31. Toniolo, A.; Olsen, S.; Manohar, L.; Martinez, T. J., Conical Intersection Dynamics in Solution: The Chromophore of Green Fluorescent Protein. *Faraday Disc.* **2004**, *127*, 149-163.
- 32. Gaenko, A.; DeFusco, A.; Varganov, S. A.; Martinez, T. J.; Gordon, M. S., Interfacing the Ab Initio Multiple Spawning Method with Electronic Structure Methods in Gamess: Photodecay of Trans-Azomethane. *J. Phys. Chem. A* **2014**, *118*, 10902-10908.
- 33. Schmidt, M. W.; Baldridge, K. K.; Boatz, J. A.; Elbert, S. T.; Gordon, M. S.; Jensen, J. H.; Koseki, S.; Matsunaga, N.; Nguyen, K. A.; Su, S.; et al., General Atomic and Molecular Electronic Structure System. *J. Comp. Chem.* **1993**, *14*, 1347-1363.
- 34. Ben-Nun, M.; Martínez, T. J., Nonadiabatic Molecular Dynamics: Validation of the Multiple Spawning Method for a Multidimensional Problem. *J. Chem. Phys.* **1998**, *108*, 7244-7257.

- 35. Press, W. H.; Teukolsky, S. A.; Vetterling, W. T.; Flannery, B. P., Numerical Recipes in Fortran. Cambridge Press: Cambridge, 1992.
- 36. Warshel, A.; Levitt, M., Theoretical Studies of Enzymic Reactions: Dielectric, Electrostatic and Steric Stabilization of the Carbonium Ion in the Reaction of Lysozyme. *J. Mol. Biol.* **1976**, *103*, 227-249.
- 37. Senn, H. M.; Thiel, W., Qm/Mm Methods for Biomolecular Systems. *Ang. Chem. Int. Ed.* **2009**, *48*, 1198-1229.
- 38. Toniolo, A.; Thompson, A. L.; Martinez, T. J., Excited State Direct Dynamics of Benzene with Reparameterized Multi-Reference Semiempirical Configuration Interaction Methods. *Chem. Phys.* **2004**, *304*, 133-145.
- 39. Owens, J. M. Theoretical Studies of the Solvation, Dynamics, and Photochemistry of Ethylene, Retinal Protonated Schiff Base, Oligocellulose, and Gd(Iii) Clusters. University of Illinois at Urbana-Champaign, Urbana, 2004.
- 40. Roos, B. O., Theoretical Studies of Electronically Excited States Using Multiconfigurational Perturbation Theory. *Acc. Chem. Res.* **1999**, *32*, 137-144.
- 41. Virshup, A. M.; Punwong, C.; Pogorelov, T. V.; Lindquist, B. A.; Ko, C.; Martinez, T. J., Photodynamics in Complex Environments: Ab Initio Multiple Spawning Quantum Mechanical/Molecular Mechanical Dynamics. *J. Phys. Chem. B* **2009**, *113*, 3280-3291.
- 42. Granucci, G.; Toniolo, A., Molecular Gradients for Semiempirical Ci Wave Functions with Floating Occupation Molecular Orbitals. *Chem. Phys. Lett.* **2000**, *325*, 79-85.
- 43. Luecke, H.; Schobert, B.; Richter, H. T.; Cartailler, J. P.; Lanyi, J. K., Structure of Bacteriorhodopsin at 1.55 Angstrom Resolution. *J. Mol. Biol.* **1999**, *291*, 899-911.
- 44. Belrhali, H.; Nollert, P.; Royant, A.; Menzel, C.; Rosenbusch, J. P.; Landau, E. M.; Pebay-Peyroula, E., Protein, Lipid and Water Organization in Bacteriorhodopsin Crystals: A Molecular View of the Purple Membrana at 1.9 Angstrom Resolution. *Struct. Fold. Des.* **1999**, *7*, 909-917.
- 45. Sasaki, J.; Lanyi, J. K.; Needleman, R.; Yoshizawa, T.; Maeda, A., Complete Identification of C=O Stretching Vibrational Bands of Protonated Aspartic Acid Residues in the Difference Infrared-Spectra of M-Intermediate and N-Intermediate Versus Bacteriorhodopsin. *Biochemistry* **1994**, *33*, 3178-3184.

- 46. Brown, L. S.; Varo, G.; Hatanaka, M.; Sasaki, J.; Kandori, H.; Maeda, A.; Friedman, N.; Sheves, M.; Needleman, R.; Lanyi, J. K., The Complex Extracellular Domain Regulates the Deprotonation and Reprotonation of the Retinal Schiff-Base During the Bacteriorhodopsin Photocycle. *Biochemistry* **1995**, *34*, 12903-12911.
- 47. Antes, I.; Thiel, W., Adjusted Connection Atoms for Combined Quantum Mechanical and Molecular Mechanical Methods. *J. Phys. Chem. A* **1999**, *103*, 9290-9295.
- 48. Toniolo, A.; Ciminelli, C.; Granucci, G.; Laino, T.; Persico, M., Qm/Mm Connection Atoms for the Multistate Treatment of Organic and Biological Molecules. *Theor. Chem. Acc.* **2004**, *111*, 270-279.
- 49. Weiner, S. J.; Kollman, P. A.; Case, D. A.; Singh, U. C.; Ghioand, C.; Alagona, G.; Jr., S. P.; Weiner, P., A New Force Field for Molecular Mechanical Simulation of Nucleic Acids and Proteins. *J. Am. Chem. Soc.* **1984**, *106*, 765-784.
- 50. Case, D. A.; Pearlman, D. A.; Caldwell, J. W.; Cheatham III, T. E.; Wang, J.; Ross, W. S.; Simmerling, C. L.; Darden, T. A.; Merz, K. M.; Stanton, R. V.; et al. *Amber 7*, University of California: San Francisco, CA, USA, 2002.
- 51. Cornell, W.; Cieplak, P.; Bayly, C.; Gould, I.; Merz, J. K.; Ferguson, D.; Spellmeyer, D.; Fox, T.; Caldwell, J.; Kollman, P., A Second Generation Force Field for the Simulation of Proteins, Nucleic Acids, and Organic Molecules. *J. Am. Chem. Soc.* **1995**, *117*, 5179-5197.
- 52. Cheatham III, T. E.; Cieplak, P.; Kollman, P. A., A Modified Version of the Cornell Et Al. Force Feld with Improved Sugar Pucker Phases and Helical Repeat. *J. Biomol. Struct. Dyn.* **1999**, *16*, 845-862.
- 53. Otomo, J., Influence Exercised by Histidine-95 on Chloride Transport and the Photocycle in Halorhodopsin. *Biochemistry* **1996**, *35*, 6684-6689.
- 54. Torrie, G. M.; Valleau, J. P., Non-Physical Sampling Distributions in Monte-Carlo Free-Energy Estimation Umbrella Sampling *J. Comp. Phys.* **1977**, *23*, 187-199.
- 55. Torrie, G. M.; Valleau, J. P., Monte-Carlo Study of a Phase-Separating Liquid-Mixture by Umbrella Sampling. *J. Chem. Phys.* **1977**, *66*, 1402-1408.
- 56. Grossfield, A. Wham-Weighted Histogram Analysis Method, 2.0.2; 2008.
- 57. Mathies, R.; Stryer, L., Retinal Has a Highly Dipolar Vertically Excited Singlet State: Implications for Vision. *Proc. Natl. Acad. Sci. U. S. A.* **1976**, *73*, 2169-73.

- 58. Birge, R. R.; Zhang, C. F., Two-Photon Spectroscopy of Light-Adapted Bacteriorhodopsin. *J. Chem. Phys.* **1990**, *92*, 7178-7195.
- 59. Kennis, J. T. M.; Larsen, D. S.; Ohta, K.; Facciotti, M. T.; Glaeser, R. M.; Fleming, G. R., Ultrafast Protein Dynamics of Bacteriorhodopsin Probed by Photon Echo and Transient Absorption Spectroscopy. *J. Phys. Chem. B* **2002**, *106*, 6067-6080.
- 60. Colonna, A.; Groma, G. I.; Martin, J. L.; Joffre, M.; Vos, M. H., Quantification of Sudden Light-Induced Polarization in Bacteriorhodopsin by Optical Rectification. *J. Phys. Chem. B* **2007**, *111*, 2707-10.
- 61. Leonard, J.; Portuondo-Campa, E.; Cannizzo, A.; van Mourik, F.; van der Zwan, G.; Tittor, J.; Haacke, S.; Chergui, M., Functional Electric Field Changes in Photoactivated Proteins Revealed by Ultrafast Stark Spectroscopy of the Trp Residues. *Proc. Natl. Acad. Sci. U. S. A.* **2009**, *106*, 7718-7723.
- 62. Schenkl, S.; van Mourik, F.; van der Zwan, G.; Haacke, S.; Chergui, M., Probing the Ultrafast Charge Translocation of Photoexcited Retinal in Bacteriorhodopsin. *Science* **2005**, *309*, 917-20.
- 63. Aharoni, A.; Khatchatouriants, A.; Manevitch, A.; Lewis, A.; Sheves, M., Protein–B-Ionone Ring Interactions Enhance the Light-Induced Dipole of the Chromophore in Bacteriorhodopsin. *J. Phys. Chem. B* **2003**, *107*, 6221-6225.
- 64. Molnar, F.; Ben-Nun, M.; Martinez, T. J.; Schulten, K., Characterization of a Conical Intersection between the Ground and First Excited State for a Retinal Analog. *J. Mol. Struct.* (*THEOCHEM*) **2000**, 169-178.
- 65. Burghardt, I.; Hynes, J. T., Excited-State Charge Transfer at a Conical Intersection: Effects of an Environment. *J. Phys. Chem. A* **2006**, *110*, 11411-11423.
- 66. Ben-Nun, M.; Molnar, F.; Schulten, K.; Martinez, T. J., The Role of Intersection Topography in Bond Selectivity of Cis-Trans Photoisomerization. *Proc. Natl. Acad. Sci. U. S. A.* **2002**, *99*, 1769-1773.
- 67. Gonzalez-Luque, R.; Garavelli, M.; Bernardi, F.; Merchan, M.; Robb, M. A.; Olivucci, M., Computational Evidence in Favor of a Two-State, Two-Mode Model of the Retinal Chromophore Photoisomerization. *Proc. Natl. Acad. Sci. U. S. A.* **2000**, *97*, 9379-9384.

- 68. Garavelli, M.; Celani, P.; Bernardi, F.; Robb, M. A.; Olivucci, M., The C5h6nh2+ Protonated Shiff Base: An Ab Initio Minimal Model for Retinal Photoisomerization. *J. Am. Chem. Soc.* **1997**, *119*, 6891-6901.
- 69. Efron, B.; Tibshirani, R., *An Introduction to the Bootstrap*; Chapman and Hall/CRC: New York and London, 1993; Vol. 57.

Table of Contents Graphic

